Structural Analysis and Assembly of the HIV-1 Gp41 Amino-Terminal Fusion Peptide and the Pretransmembrane Amphipathic-At-Interface Sequence†

Maier Lorizate,‡ Igor de la Arada,‡ Nerea Huarte,‡ Silvia Sánchez-Martínez,‡ Beatriz G. de la Torre,§ David Andreu,§ José L. R. Arrondo,‡ and José L. Nieva*,‡

Biophysics Unit (CSIC-UPV/EHU) and Biochemistry Department, University of the Basque Country, P.O. Box 644, 48080 Bilbao, Spain, and Proteomics Unit, Pompeu Fabra University, Dr. Aiguader 80, 08003 Barcelona, Spain

Received June 23, 2006; Revised Manuscript Received September 28, 2006

ABSTRACT: The amino-terminal region within the HIV-1 gp41 aromatic-rich pretransmembrane domain is an amphipathic-at-interface sequence (AIS). AIS is highly conserved between different viral strains and isolates and recognized by the broadly neutralizing 2F5 antibody. The atomic structure of the native Fab2F5-bound AIS appears to involve a nonhelical extended region and a β-turn structure. We previously described how an immunogenic complex forms, based on the stereospecific interactions between AIS and the gp41 amino-terminal fusion peptide (FP). Here, we have analyzed the structure generated by these interactions using synthetic hybrids containing AIS and FP sequences connected through flexible tethers. The monoclonal 2F5 antibody recognized FP−AIS hybrid sequences with an apparently higher affinity than the linear AIS. Indeed, these hybrids exhibited a weaker capacity to destabilize membranes than FP alone. A combined structural analysis, including circular dichroism, infrared spectroscopy, and two-dimensional infrared correlation spectroscopy, revealed the existence of specific conformations in FP−AIS hybrids, predominantly involving β-turns. Thermal denaturation studies indicated that FP stabilizes the nonhelical folded AIS structure. We propose that the assembly of the FP−AIS complex may act as a kinetic trap in halting the capacity of FP to promote fusion.

The gp120/41 envelope glycoprotein of the human immunodeficiency virus-1 (HIV-1)[1] promotes fusion between the viral envelope and the plasma membrane of the $CD4^+$ target cell (*1*−*3*). The triggering of fusion involves the binding of the surface gp120 subunit to CD4 and human chemokine receptors. Subsequently, coupled to the refolding of its globular ectodomain, the transmembrane gp41 subunit promotes the initial apposition and then the merging of the lipid bilayers. According to the resolved atomic structure (*4*, *5*), the ectodomain end product consists of a thermodynamically stable trimeric six-helix bundle (6-HB). In the 6-HB "hairpinlike" configuration, the carboxy-terminal helices (CHR) pack in the reverse direction, against the hydrophobic grooves that are outside of a trimeric coiled-coil assembly involving the amino-terminal helical regions (NHR) (*4*, *5*). The fact that CHR peptides can readily inhibit fusion suggests that the trimeric NHR core is accessible to solvent in a "prehairpin" configuration (*6*−*8*). Formation of the 6-HB also brings the amino-terminal fusion peptide (FP) and the transmembrane domain (TMD) closer to each other, pointing toward the same lipid bilayer.

Given the FP's hydrophobic character, it has been postulated that prior to 6-HB formation, the FP inserts into the target cell membrane where it generates the specific perturbations required for catalysis of the merging of the membranes (reviewed in ref *9*). On the basis of mutational analyses and their strong propensity for partitioning into membrane interfaces, the pretransmembrane domain (preTM, also designated as MPER: membrane proximal external region) has been predicted to participate in this process by inserting into the membrane (*10*−*16*). Thus, it has been inferred that 6-HB formation would bring the two membranes primed for fusion into apposition (*12*).

To date, the atomic structure of the prefusion gp41 ectodomain remains unknown. Recent cryoelectron microscope tomography study in virions has revealed that the gp41 stalk region projects like a "leg" from the trimeric Env complex (*17*). This structure forms a "foot" just above the plane of the viral envelope believed to contain the membrane proximal external sequences that are recognized by neutralizing antibodies. On the basis of the prediction that preTM and FP may be found in proximity in a prefusion gp41 state, we have recently explored the possibility that contacts between both regions may stabilize an immunogenic stemlike complex (*18*). The monoclonal 2F5 antibody (mAb2F5) (*19*, *20*) was used to determine whether stereospecific interactions between FP and membrane proximal residues might stabilize a nativelike structure recognized by the antibody. The linear 2F5 epitope sequence was extended to incorporate residues

† This study was supported by Spanish Ministerio de Educación y Ciencia (BFU 2005-0695) and University of the Basque Country (042.310-13552/2001). M.L. was a recipient of a predoctoral fellowship of the Basque Government.

* To whom correspondence should be addressed: Biophysics Unit (CSIC-UPV/EHU) and Biochemistry Department, University of the Basque Country, P.O. Box 644, 48080 Bilbao, Spain. Phone: 34 94 6013353. Fax: 34 94 6013360. E-mail: gbpniesj@lg.ehu.es.

‡ University of the Basque Country.

§ Pompeu Fabra University.

[1] Abbreviations: AIS, amphipathic-at-interface sequence; CD, circular dichroism; FP, fusion peptide; HIV, human immunodeficiency virus; IR, infrared stectroscopy; mAb, monoclonal antibody.

10.1021/bi0612521 CCC: $33.50
Published on Web 11/09/2006

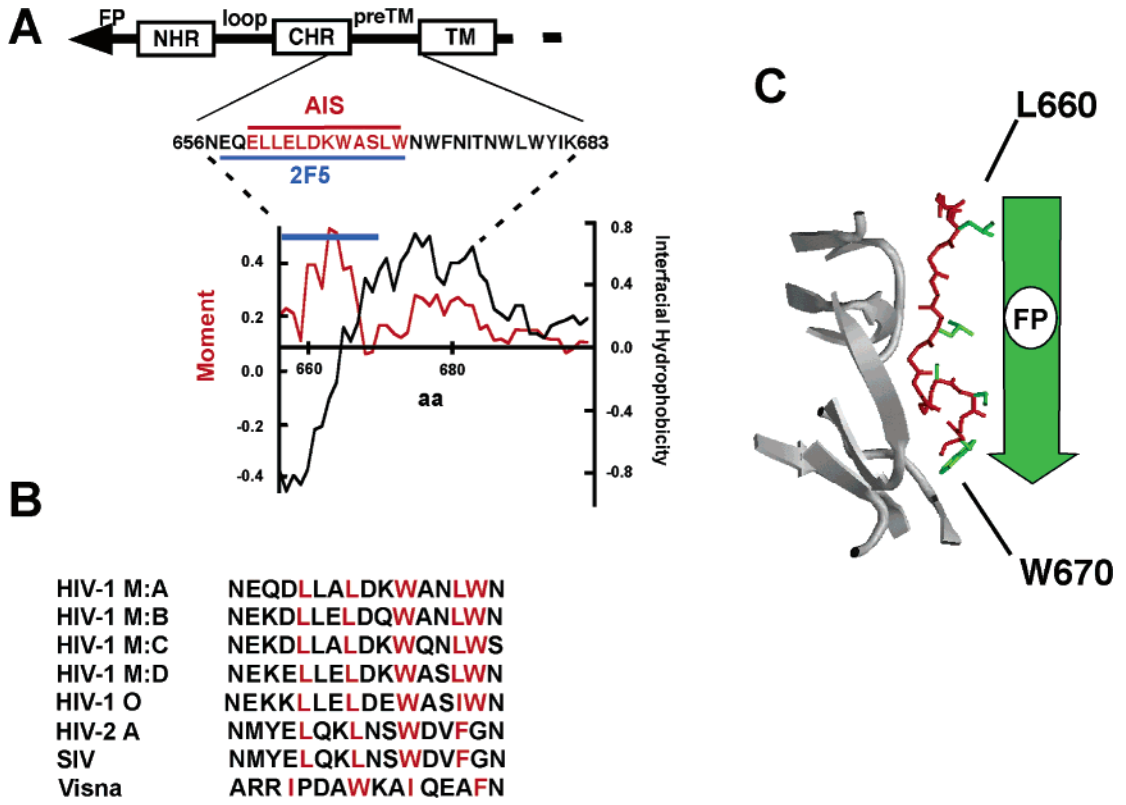

FIGURE 1: (A) Designation of gp41 amphipathic-at-interface (AIS) pretransmembrane sequence (sequence colored red). The plot compares for a window of 11 amino acids hydrophobicity-at-interface (black trace, mean values of free energies of transfer from membrane interfaces to water) and hydrophobic-at-interface moment [red trace, mean moment of a fixed δ of 100°, calculated as described by Sáez-Cirión et al. (*14*)]. The plotted stretch encompasses the Env sequence of residues 656−700 (based on the BH10 isolate with GenBank entry M15654). Free energy values for individual residues were obtained in both cases from the Wimley−White scale (*54*). The region spanned by the 2F5 epitope is denoted with the blue line. The regions designated in the diagram include FP (fusion peptide), NHR and CHR (amino- and carboxy-terminal helical regions, respectively), preTM (pretransmembrane), and TM (transmembrane domain). (B) Multiple-sequence alignment of lentivirus AIS domains using CLUSTALW. Hydrophobic residues with affinity for the membrane interface are colored red. Representative sequences were obtained from refs *14* and *55*. (C) Structure of $_{657}$EQELLELDKWASLW$_{670}$ bound to Fab2F5 (red chain and ribbons, respectively). The side chains of L660, L663, A667, S668, and W670 (green) are shown oriented toward the nonbound surface. The green arrow represents the putative region occupied by amino-terminal FP residues adopting an unknown structure. The AIS structure [derived from Protein Data Bank entry 1TJI (*23*)] was rendered with Swiss-PDBviewer.

Table 1: Peptide Sequences Used in This Study

name	sequence	Gp160 numbering[a]
FP_n	AVGIGALFLGFLGAAG	512−527
FPK3	AVGIGALFLGFLGAAGSTMGARSKKK	512−534-KKK
AIS[b]	NEQELLELDKWASLWN	656−671
preTM	DKWASLWNWFNITNWLWYIK	664−683
Hyb	AVGIGALFLGFLGAAG-Ahx-NEQELLELDKWASLWNC	512−527-Ahx-656−671-C
HybK3	GIGALFLGFLGAAGSKK-Ahx-KNEQELLELDKWASLWN	514−528-KK-Ahx-655−671

[a] Numbering based on the BH10 isolate (GenBank entry M15654). [b] Designated 2F5ep in our previous study (*18*).

that might improve antibody recognition (*21*−*23*), including the conserved membrane proximal region that we previously defined as an amphipathic-at-interface sequence (AIS, Figure 1; *14*). Critical specificity controls, which included the use of scrambled FP versions and sequences with two conserved Phe residues exchanged with their D-stereoisomers, demonstrated the structure-specific conformational effects of FP on the AIS region (*18*).

Thus, we concluded that stereospecific FP−AIS interactions might stabilize the gp41 stem region in a prefusion state (*18*). Here, we have used hybrid peptides that combine the AIS and FP sequences through flexible tethers to analyze the structures involved in those interactions. Not only were single hybrid species recognized by mAb2F5 with an affinity higher than that of the linear epitope, but they restrained FP-induced membrane perturbations and were enriched in β-turn and β-sheet structures. Thus, our results provide evidence that FP and AIS may assemble into a complex that could confer solubility to the membrane proximal gp41 stem region. Within this complex, the CHR C-terminus is retained in a nonhelical conformation and the 2F5 epitope is configured as a prefusion structure. On the basis of these results and recently reported ultrastructural data (*17*), we propose a model that explains the implications of FP−AIS interactions in gp41 refolding during fusion.

MATERIALS AND METHODS

Materials. The peptides listed in Table 1 were synthesized in C-terminal carboxamide form by solid-phase methods using Fmoc chemistry and purified by HPLC (purity of

>95%). Peptides were dissolved in dimethyl sulfoxide (DMSO, spectroscopy grade) and their concentrations determined by the biscinchoninic acid microassay (Pierce, Rockford, IL). *N*-(7-Nitrobenz-2-oxa-1,3-diazol-4-yl)phosphatidylethanolamine (*N*-NBD-PE), *N*-(lissamine rhodamine B sulfonyl)phosphatidylethanolamine (*N*-Rh-PE), and 1-palmitoyl-2-oleoylphosphatidylglycerol (POPG) were purchased from Avanti Polar Lipids (Birmingham, AL). 8-Aminonaphthalene-1,3,6-trisulfonic acid sodium salt (ANTS) and *p*-xylenebis(pyridinium)bromide (DPX) were from Molecular Probes (Junction City, OR). mAbs 2F5 and 4E10 were purchased from Polymun Inc. (Vienna, Austria). CHO-Env cell lines (contributed by C. Weiss and J. White) and HeLa cell lines (contributed by R. Axel) were obtained from the National Institutes of Health AIDS Research and Reference Reagent Program (ARRRP).

Blockage of Syncytium Inhibition. The syncytium assay was carried out using CHO-Env cells (ARRRP, generated by C. Weiss and J. White) and HeLaT4+ cells expressing CD4 and CXCR4 (ARRRP, generated by R. Axel). The inhibition assay was performed as described previously (*18*).

Membrane Stability. The capacity of FP to destabilize large unilamellar POPG vesicles was assayed using previously described methods (*24*). Release of vesicular contents into the medium was monitored by the ANTS/DPX assay (*25*) and fusion as the mixing of their membrane components, and it was monitored by the resonance energy transfer assay [RET assay (*26*)].

Circular Dichroism. Circular dichroism (CD) measurements were obtained from a thermally controlled Jasco J-810 circular dichroism spectropolarimeter calibrated routinely with (1*S*)-(+)-10-camphorsulfonic acid, ammonium salt. Stock peptide samples consisted of single sequences or mixtures preincubated in DMSO, lyophilized, and finally dissolved in 2 mM Hepes (pH 7.4) at concentrations between 0.03 and 0.3 mM. Spectra were measured in a 1 mm path length quartz cell initially equilibrated at 25 °C. Data were taken with a 1 nm bandwidth at a speed of 20 nm/min, and the results of five scans were averaged.

Infrared Spectroscopy. Infrared spectra were recorded in a Bruker Tensor 27 spectrometer equipped with a mercury−cadmium−telluride detector using a Peltier-based temperature controller (TempCon, BioTools Inc., Wauconda, IL) with calcium fluoride cells (BioCell, BioTools Inc.). Typically, 1000 scans were collected for each background and sample, and the spectra were obtained with a nominal resolution of 2 cm^{-1}. Data treatment and band decomposition of the original amide I have been described elsewhere (*27*, *28*). To obtain the two-dimensional IR maps, modification of the HFIP concentration was used to induce spectral fluctuations and to detect dynamic spectral variation in the secondary structure of hybK3. Rendering of the two-dimensional synchronous and asynchronous spectra has been described previously (*29*).

RESULTS

The Neutralizing 2F5 Antibody Recognizes the Conserved AIS Region. A simultaneous computation of interfacial hydrophobicity and the hydrophobic-at-interface moment (*14*) revealed that the high-affinity linear epitope recognized by mAb2F5 and the amphipathic-at-interface sequence connecting gp41 CHR and preTM domains practically coincide (Figure 1A). AIS was proposed to play a role as an interface helical connector (*14*). Indeed, the amphipathic characteristics of the AIS region as a helix are highly conserved across the different HIV-1 strains and clinical isolates (panel B), even though the sequence diverges in other members of the Lentiviridae family. Nevertheless, the overall amphipaticity at interface is maintained for all family members, suggesting that selective pressure has preserved this structural motif.

The prefusion AIS structure may actually be inferred from the Fab2F5-bound epitope sequence, which was resolved through X-ray diffraction (*23*) (Figure 1C). The most prominent structural features of the prefusion AIS included (i) the nonhelical conformation consisting of a combination of extended elements and β-turns and (ii) the existence of an unbound hydrophobic surface that must contact other portions of gp41. We have reported that FP residues orient and/or stabilize AIS, and therefore, they increase the affinity of mAb2F5 (*18*). Thus, we speculate that FP interacts with and stabilizes the AIS native structure as proposed in the model depicted in Figure 1C. We note here that the HIV-1 FP structures available at the Protein Data Bank (entries 1ERF and 2ARI) would not be relevant for this model since they pertain to monomeric species immersed in a nonpolar environment; i.e., they represent a membrane-inserted version of the sequence, most likely produced upon fusion activation (refs *30* and *31*; see also the Discussion).

mAb2F5 Recognizes FP−AIS Hybrids with Higher Affinity. To analyze the structures that might originate as a consequence of the specific FP−AIS interactions, we have combined both domains into single hybrid species (Table 1). First, we tested whether the FP-containing hybrid constitutes a more precise representation of the native epitope recognized by mAb2F5, comparing the antibody affinities for the linear AIS epitope, AIS/FP_n mixtures, and the "hyb" peptide (as displayed in Table 1). Adsorption of mAb2F5 was promoted both in the mixtures and even more intensely when the hyb peptide was applied to the plaques. This result is consistent with the FP stretch in the hyb peptide enhancing epitope recognition (Figure 2A, left). Control experiments demonstrated that the presence of FP did not appreciably affect the binding of mAb4E10 (*32*), an antibody that recognizes a downstream preTM sequence (Figure 2A, right).

The affinity of mAb2F5 was also assessed in solution, as inferred from the peptide's ability to interfere with antibody recognition of functional gp41 expressed on the cell surface (Figure 2B). All the formulations that were tested reversed the mAb2F5-induced blockage of syncytium formation (micrographs on the left). This inhibitory effect was dose-dependent in all cases, indicating that the FP_n/AIS mixture and hyb were more efficient formulations than AIS (panel B, right). Hence, these data again suggest that both FP-stabilized sequences better emulate the native gp41 2F5 epitope than the linear epitope alone.

The FP Sequence Exhibits Less Membrane Activity within the FP−AIS Hybrid. We next examined the capacity of FP as a part of the hybrid to compromise the integrity of the bilayer and promote fusion. The interaction of the HIV-1 FP sequence with negatively charged phosphatidylglycerol has been shown to form permeabilizing pores in lipid vesicles, while the addition of Ca^{2+} promotes peptide-induced

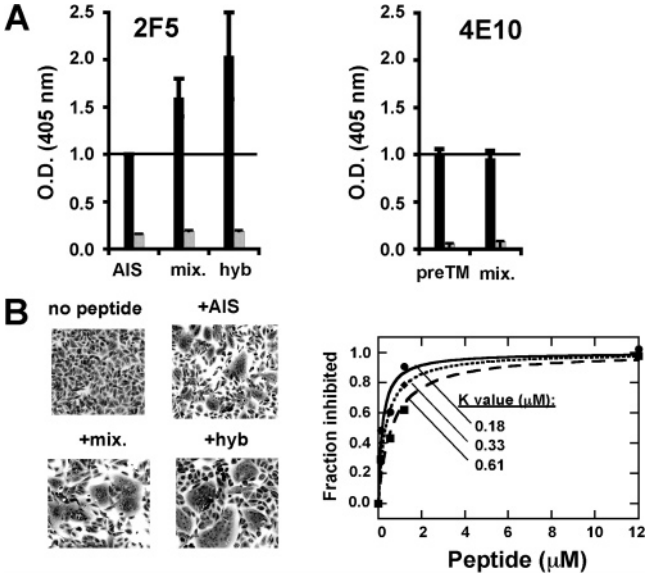

FIGURE 2: Increase in the mAb2F5 reactivity in the presence of FP and hybrid sequences. (A) Peptide-based ELISAs: (left) mAb2F5 (0.075 μg/mL) binding to plates coated with AIS alone, a FP_n/AIS (equimolar ratio) mixture (mix.), and hyb peptide and (right) mAb4E10 (0.3 μg/mL) binding to plates coated with preTM alone and FP_n/preTM equimolar mixtures (mix.). In both cases, peptides were applied to the plates at a concentration of 1.4 μM. BSA signals (AIS, hyb, and preTM samples) and those of FP_n alone (mix. samples) are also shown (hatched columns). (B) Binding in solution based on gp41 fusion activity recovery by preincubation of mAb2F5 with peptides. As the left, cells grown in 96-well plates were treated with mAb2F5 (5 μg/well). mAb was preincubated with either AIS, an equimolar FP_n/AIS mixture (mix.), or hyb (1.2 μM) as indicated. In control samples with no peptide (100% blocking activity), the mAb was incubated with the same amount of DMSO. At the right, the dose dependency of inhibition of mAb2F5 (5 μg/well) by preincubation with the AIS (-■-), the mixture (—●—), or the hyb peptide (···◆···) is given; 100% inhibition was established as the number of nuclei present in syncytial plaques (fused cells containing four or more nuclei) per field, in the absence of mAb2F5. Means of duplicate points in representative experiments are displayed. Half-maximal binding values (*K*) were inferred by fitting experimental values to hyperbolic functions.

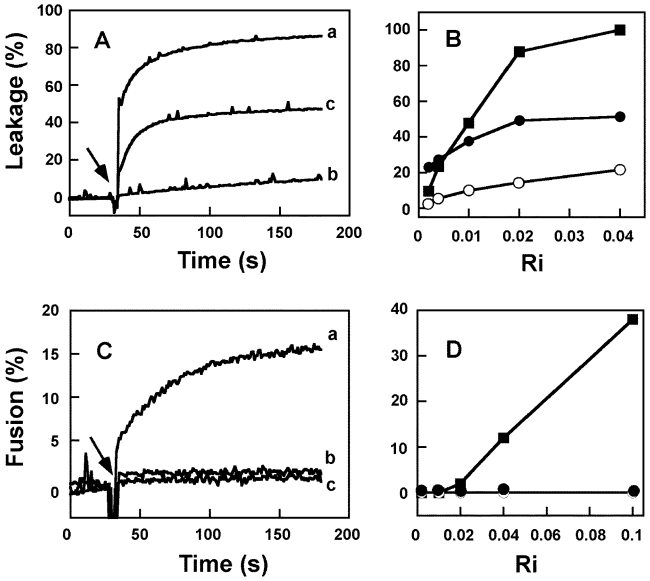

FIGURE 3: Bilayer destabilizing activity of the hybrid sequence measured in POPG large unilamellar vesicles. (A) Kinetics of leakage of vesicular contents (ANTS/DPX assay) at a 1:50 peptide:lipid ratio induced by FP_n (a), AIS (b), and hyb (c). The peptide was added at the time indicated by the arrow. The lipid concentration was fixed at 50 μM. (B) Final extent of the leakage process as a function of the molar peptide:lipid ratio (R_i) induced by FP_n (■), AIS (○), and hyb (●). (C) Kinetics of intervesicular mixing of lipids induced at a 1:25 peptide:lipid ratio by FP_n (a), AIS (b), and hyb (c). The peptide was added at the time indicated by the arrow. The lipid concentration was fixed at 100 μM, and the assay was carried out in the presence of 5 mM calcium. (D) Final portion of the lipid mixing process plotted as a function of the peptide:lipid ratio. Symbols are as in panel B.

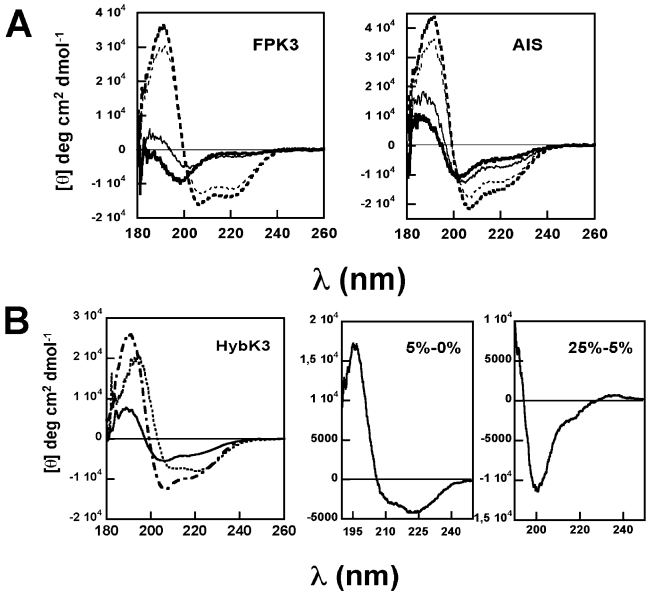

FIGURE 4: CD characterization of FPK3, AIS, and hybK3 sequences. (A) Far-UV CD spectra of FPK3 and AIS with varying amounts of HFIP. The percentage (v/v) of HFIP in the samples was 0 (thick solid line), 5 (thin solid line), 12.5 (thin dashed line), and 25% (thick dashed line). (B) HybK3 spectra measured in 0 (solid line), 5 (dotted line), and 25% (dashed line) HFIP (v/v). The middle and right panels display 5% − 0% and 25% − 5% difference spectra, respectively.

fusion by supporting liposome aggregation [i.e., cation-assisted fusion (*24*, *33*)]. Thus, we compared the abilities of FP_n, AIS, and hyb to permeabilize and fuse vesicles (Figure 3). FP_n effectively permeabilized liposomes at increasing peptide concentrations and induced the merging of bilayers in the presence of Ca^{2+}. In comparison, the AIS region did not induce a significant release of the aqueous contents of liposomes, and it was unable to induce vesicle fusion. As a component of the hyb peptide, the capacity of FP to induce permeabilization was also diminished while its fusogenic influence was completely abolished. Thus, the FP−AIS interactions appear to reduce the capacity of FP to perturb membranes.

FP Stabilizes a Nonhelical Conformation of the AIS. The observation that mAb2F5 recognized the FP−AIS hybrid with higher affinity suggests that interactions between these sequences favored specific conformations more closely related to the native structure of the 2F5 gp41 epitope. The combined CD−IR spectroscopic study described below supports the existence of a stable FP−AIS complex with a specific β-turn- and β-sheet-rich secondary structure (Figures 4−8). As mentioned in the introductory section, a FP−AIS complex might be located close to the viral membrane surface (*17*). Thus, we also analyzed the structural effect of a polarity gradient similar to that existing at the bilayer interface using 1,1,1,3,3,3-hexafluoro-2-propanol (HFIP). HFIP was particularly useful in studying the in-solution

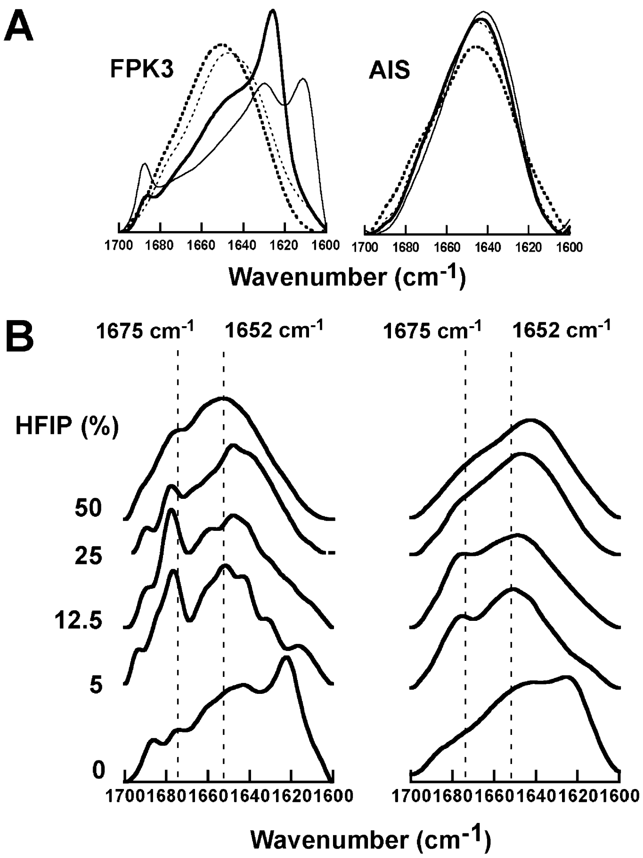

FIGURE 5: IR characterization of FPK3, AIS, and hybK3 sequence. (A) Amide I region IR spectra, measured in D_2O-based PBS buffer, of FPK3 and AIS with various amounts of HFIP. The HFIP concentration (v/v) in the samples was 0 (thick solid line), 5 (thin solid line), 12.5 (thin dashed line), and 25% (thick dashed line). (B) Original (right) and Fourier self-deconvolved (left) IR spectra of hybK3 in the amide I region with various amounts of HFIP as indicated.

assembly of individual FP and AIS regions (*18*). Moreover, HFIP is the alcohol that more closely mimics the bilayer structuring effects on the FP sequence (*30*).

Using CD spectroscopy, we first examined the structure of the hyb constituents separately (Figure 4A). The soluble FPK3 derivative exhibited negative bands at or below 200 nm and a weaker negative component between 220 and 230 nm, indicating that this derivative did not adopt a predominant secondary structure in the buffer (left panel). Slightly different AIS spectra were collected under the same experimental conditions, with a shift of the minimum to longer wavelengths together with weak negative shoulders at ≈220 nm (right panel). These spectra essentially reproduced the pattern in water at 400 μM described for a similar peptide associated with predominant 3_{10}-helical conformation (*34*). Subsequently, this same type of spectrum was interpreted as arising from an ensemble of conformations including turn and helical structures (*22*). HFIP induced the appearance of double minima at 208 and 222 nm in both samples and an increasingly stronger positive absorption at ca. 190 nm, compatible with an increase in α-helix content (*35, 36*).

CD analysis was then performed on "hybK3", a soluble derivative of the hybrid sequence (Table 1). The hybK3 peptide retains the FP core residues, and it incorporates three additional Lys residues, one of which corresponds to the Lys655 preceding the AIS in the HIV-1 Env sequence. When applied to plates, hybK3 was better recognized by mAb2F5 than the lineal AIS epitope (not shown), confirming that the FP core can orient the linear epitope. In buffer, hybK3 essentially exhibited an identical CD spectrum within the 0.03–0.3 mM range, with negative bands centered at ≈202–205 nm, a negative shoulder at ≈224 nm, and positive absorption at 190 nm (Figure 4B). The hybK3 spectrum changed in 5% HFIP, exhibiting a red-shifted positive band together with a $[\theta]_{222}/[\theta]_{208}$ ellipticity ratio of >1. These features were not observed in FPK3 or AIS samples, suggesting that the specific conformations adopted by hybK3 originated from the interactions between its constituent sequences. In principle, these spectra are characteristic of peptides with a high α-helix content [Table 2; see also the 5% – 0% difference spectrum (middle panel)], supporting the existence of helix–helix interactions as described for heterodimeric coiled coils (*37*, *38*). However, the possibility that conformers containing a considerable population of type I β-turns could give rise to similar CD spectra cannot be excluded (*39*, *40*; see also the IR data below). In 25% HFIP, the hybK3 spectra coincided with those of the isolated FPK3 and AIS peptides. The positive band had reverted to 190 nm, and when considered together with the $[\theta]_{222}/[\theta]_{208}$ ratio of <1, this might reflect a disruption of the helix–helix interactions (*38*). The 25% – 5% difference spectrum revealed a contribution from unordered conformations as the proportion of HFIP increased, suggesting the presence of single and/or more flexible helices in 25% HFIP samples (see also the values listed in Table 2).

The CD-based conformational characterization was improved by adding IR spectroscopy data (Figures 5 and 6 and Table 3). IR samples were measured at concentrations ranging between 0.75 and 4 mM. Within this concentration range, the FPK3 amide I band exhibited two prominent features characteristic of intermolecular β-sheet structures, centered at 1624 and 1687 cm^{-1} (Figure 5A, left) (*27*, *28*). The presence of increasing amounts of HFIP induced two effects: reduction of the intermolecular bands and structuring. In 25% HFIP, the spectrum exhibited a maximum at 1650 cm^{-1}, in accordance with the HFIP-induced increase in α-helix content. In comparison, the AIS spectrum in buffer displayed a broad peak centered at ca. 1645 cm^{-1} consistent with a predominance of irregular and unordered structures (*27*, *28*). The maxima in 12.5 and 25% HFIP spectra were slightly shifted toward higher wavenumbers.

The IR spectra for hybK3 reflected the structural changes that originated from the interaction between FP and AIS (FIgure 5B and Table 3). In buffer, a band at 1620 cm^{-1} was much less intense than in FPK3. For the rest of the amide I band, the components centered at 1633 cm^{-1} (β-sheet) and 1674/1662 cm^{-1} (β-turns/β-sheet/3_{10}-helix) accounted for 75% of the spectrum area that can be attributed to periodic structures, while there was a minor contribution from a band centered at 1650 cm^{-1} (α-helix, Table 3). At a low HFIP content (5 and 12.5%) a band centered at ≈1676 cm^{-1} became predominant, although it was not a major component in the corresponding FPK3 and AIS samples. This band might be assigned to β-turns. Additionally, the contribution of the component at 1633–1630 cm^{-1} (β-sheet) diminished (Table 3). The 1676–1678 cm^{-1} band gradually disappeared at increasing HFIP concentrations as the bands at 1663–1664 cm^{-1} (turns or 3_{10}-helix) and 1650 cm^{-1} (α-helix) were

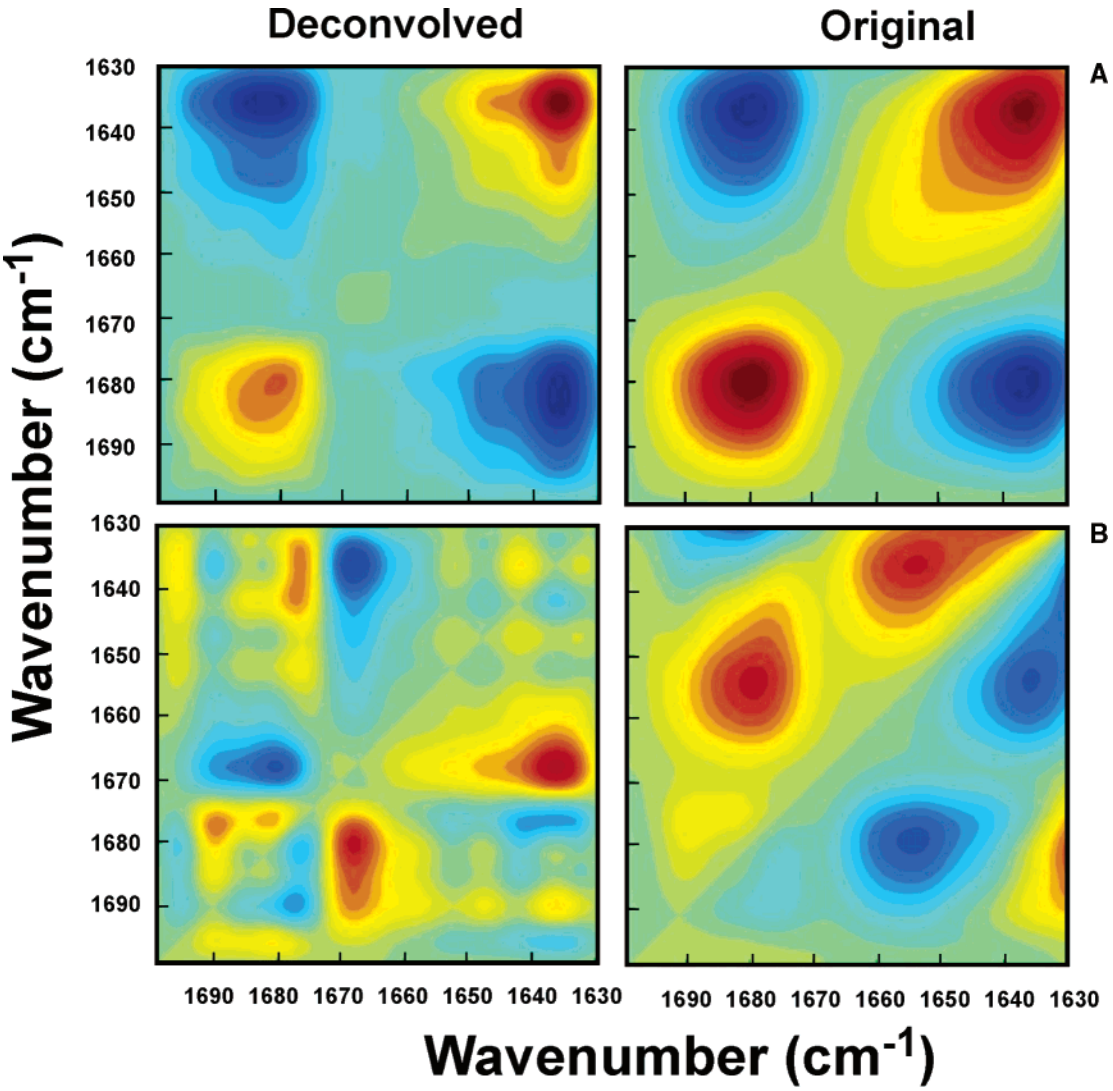

FIGURE 6: Synchronous (A) and asynchronous (B) correlation map contour in the 1700−1630 cm^{-1} interval of the original hybK3 IR (right) and Fourier self-deconvolved (left) spectra displayed in Figure 5. The contributions of the bands at 1622 and 1685 cm^{-1} in 0% HFIP samples were not taken into account for the analysis. Red peaks correspond to positive correlations and blue peaks to negative ones.

augmented in weight (Table 3). The spectrum recorded with 50% HFIP was broad and centered at 1652 cm^{-1}, and it exhibited contributions consistent with an increased level of intrinsic disorder and principally an α-helical conformation (Table 3).

Thus, the combined CD and IR hybK3 data (Figures 4 and 5 and Tables 2 and 3) suggested that FP−AIS interactions involved nonhelical β-turn/β-sheet structures. These structures were further analyzed by two-dimensional IR (Figure 6). This approach uses a correlation analysis of the dynamic fluctuations caused by an external perturbation to enhance the spectral resolution without assuming any line shape model for the bands (*41*). As previously pointed out, in our case the external perturbation consisted in the HFIP-induced gradual decrease of the medium polarity. In the synchronous two-dimensional maps (top panels), the peaks located along the diagonal (autopeaks) correspond to changes in intensity induced by the perturbation, and they were always positive. The cross-relation (nondiagonal) peaks indicate an in-phase relationship between the two bands that are involved; i.e., two vibrations of the peptide characterized by two different wavenumbers (ν_1 and ν_2) were simultaneously affected (*42, 43*). Asynchronous maps (bottom panels) show the not-in-phase cross-relation peaks between the bands and give an idea of the sequential order of events produced by the perturbation (i.e., an asynchronous peak is produced when the vibrations of the functional groups corresponding to the varying wavenumbers change at different times). The asynchronous peak will be positive if the change in ν_1 occurs earlier than that in ν_2, and negative if otherwise.

When considering original hybK3 spectra not including the intermolecular bands (right panels), the synchronous plot exhibited autopeaks at ca. 1680 and 1635 cm^{-1}, indicating that β-turns and β-sheets would be the main structures affected by the change in polarity. A negative cross-correlation peak was found for the 1635/1680 cm^{-1} band pair, consistent with the peak intensities displaying a contrasting behavior after the change in polarity (i.e., that at 1680 cm^{-1} increases whereas that at 1635 cm^{-1} decreases; see Table 3). The asynchronous plot exhibited positive correlation peaks for the 1655/1680 and 1635/1655 cm^{-1} pairs. Since the 1655/1680 cm^{-1} region in the synchronous peak was negative, the positive correlation in the asynchronous map was actually established for the inverse 1680/1655 cm^{-1} pair. In conjunction, the presence of both peaks

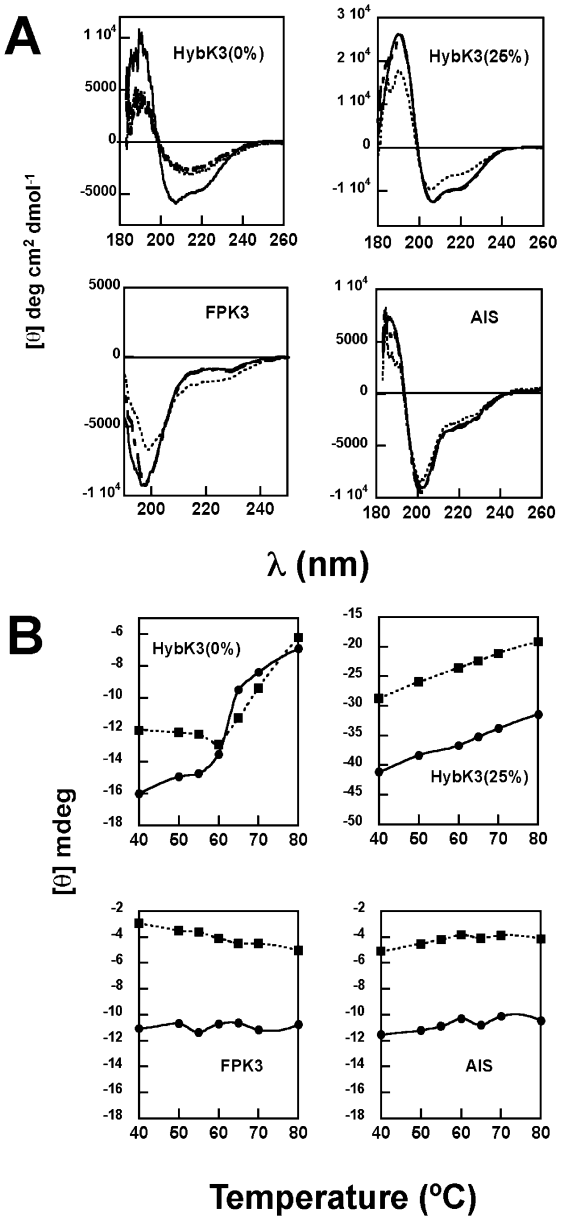

FIGURE 7: Thermal denaturation of hybK3. (A) Effect of heat on the conformation adopted by the different peptides. Spectra were measured at 25 (solid lines) and 70 °C (dotted lines). Dashed lines correspond to spectra recorded after the samples had cooled to 25 °C. The peptide concentration was 100 μM. (B) CD thermal profiles recorded at 205 (—●—) and 220 nm (-■-). Peptide samples (indicated in the panels) were ramped from 25 to 80 °C and allowed to equilibrate for 5 min at each temperature before the spectra were recorded.

suggests that nonhelical β-turns and β-sheets gave rise to helical structures with a decrease in medium polarity.

The asynchronous plot using deconvolved spectra (left panels) revealed the presence of additional peaks, positively correlated as follows: 1675/1635, 1675/1690, 1675/1666, and 1635/1666 cm^{-1}. The presence of these pairs suggests that changes in the β-turn band at 1675 cm^{-1} precede those at β-sheet 1635 and 1690 cm^{-1} bands, and changes in both structures precede those that occur in the band at 1666 cm^{-1} assigned to turns or the 3_{10}-helix (*40*, *44*−*46*). In summary, two-dimensional IR results suggested the existence of nonhelical β-turn FP−AIS conformations, which were stable at moderate low polarity and that eventually evolved toward helices in media with increasing HFIP contents.

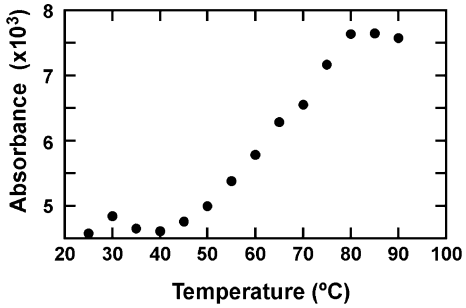

FIGURE 8: Thermal profile of the hybK3 1624 cm^{-1} amide I band intensity. Thermal analysis was performed in the 25−90 °C interval in 5 °C steps.

Table 2: HybK3 Secondary Structure Fractions Estimated from the CD Spectra Displayed in Figure 4B Using CDPro (*53*)[a]

structure	0% HFIP	5% HFIP	25% HFIP
helix (r/d)	0.088/0.097	0.229/0.154	0.210/0.146
	0.030/0.034	0.236/0.155	0.140/0.102
	−/−	0.172/0.126	−/−
strand (r/d)	0.207/0.105	0.127/0.069	0.127/0.089
	0.240/0.066	0.133/0.092	0.176/0.097
	−/−	0.098/0.079	−/−
turn	0.196	0.187	0.159
	0.209	0.179	0.209
	−/−	0.233	−
unordered	0.308	0.234	0.268
	0.409	0.179	0.276
	−/−	0.233	−

[a] Fractions estimated with CONTIN-LL, CDSSTR, and SELCON3 (top, middle, and bottom values, respectively). The SP29 reference protein set provided by the software was used for calculating the reconstructed spectra.

In the search for a putative stable ensemble of the initial conformations, the thermal stabilities of FPK3, AIS, and hybK3 were compared (Figure 7). The hybK3 CD spectrum underwent an irreversible change at high temperatures characterized by reduced absorption and minimum definition at ca. 215 nm (panel A). Importantly, a comparable heat-induced irreversible hybK3 change was observed with 5% HFIP (not shown), but not with 25% HFIP. In contrast, heating did not induce significant changes in AIS. The FPK3 sample displayed a gradual decrease in overall absorption consistent with greater thermal motion. Moreover, the changes observed in this case were reversed with cooling.

The heat-induced spectral changes conformed with the adoption of extended structures that accompany unfolding and aggregation. In support of this possibility, the thermal profiles in panel B showed that a cooperative transition between two conformational states occurred only with hybK3 in buffer, giving a T_m of approximately 60−65 °C. This thermal transition was subsequently confirmed by IR, as reflected by the increase in the intensity of the 1620 cm^{-1} intermolecular band (Figure 8). Together, these features were indicative of thermal denaturation and implied the presence of an initial folded state for hybK3 in solution.

DISCUSSION

The FP−AIS Interaction Stabilizes Type I β-Turn Structures. Our results support two effects that originate in the combination of FP and AIS domains in a hybrid peptide: (i) restraining the well-established capacity of FP to perturb membranes and (ii) stabilization of the nonhelical structures

Table 3: Band Position, Assignment, and Percent Area of the Components Obtained after Curve Fitting of IR Spectra Displayed in Figure 5B[a]

0% HFIP		5% HFIP		12.5% HFIP		25% HFIP		50% HFIP	
band position[b]	area (%)[c]	band position[b]	area (%)[c]	band position[b]	area (%)[c]	band position[b]	area (%)[c]	band position[b]	area (%)[c]
1674 (β-turns)	15	1676 (β-turns)	32.5	1678 (β-turns)	23	1678 (β-turns)	15	1681 (β-turns)	6
1662 (β-turn/3_{10}-helix)	18	1662 (β-turn/3_{10}-helix)	9	1663 (β-turn/3_{10}-helix)	25	1664 (β-turn/3_{10}-helix)	22	1668 (β-turn/3_{10}-helix)	24
1652 (α-helix)	20	1653 (α-helix)	25.5	1650 (α-helix)	24	1650 (α-helix)	31	1649 (α-helix)	36
1643 (unordered)	20	1642 (unordered)	15	1640 (unordered)	17	1638 (unordered)	21	1633 (unordered+ β-sheet)	34
1633 (β-sheet)	27	1631 (β-sheet)	18	1630 (β-sheet)	11	1629 (β-sheet)	11		

[a] Intermolecular bands centered at 1624 and 1687 cm^{-1} were not included in the calculations. [b] Wavenumbers in inverse centimeters. The conformation assigned for each position is indicated below. [c] The values have been rounded off to the nearest integer.

that are relevant for recognition by mAb2F5. The prefusion AIS atomic structure (ref *23* and Figure 1C) includes an extended conformation at the amino terminus, followed by two consecutive type I β-turns. The latter structures involve the carboxy-terminal DKWA and WASL residues that play a crucial role in antibody recognition (*47*−*49*). AIS structure only displays three intrapeptide hydrogen bonds that constrain the carboxy-terminal epitope core region of residues 664−667. Hence, in solution, this region is weakly constrained into the conformation recognized by the antibody (discussed in ref *23*). Our CD and IR data confirmed the conformational flexibility of the AIS (*22*, *34*, *50*) and FP (reviewed in ref *9*) sequences. In addition, our results suggest that this intrinsic flexibility allows them to fold into a more stable structure that is better recognized by mAb2F5.

Combining CD and IR studies aided in the elucidation of the structures that evolve from the FP−AIS interactions. The CD spectrum of hybK3 in buffer, characterized by a reduced $[\theta]_{222}/[\theta]_{208}$ ratio, resembles those of model peptides emulating 3_{10}-helices or type I β-turns (*39*, *40*, *45*, *46*) or those of type II β-rich proteins (*36*). Supporting nonhelical structures, the IR spectrum was enriched in β-turn and β-sheet conformations. Slightly decreasing the polarity of the medium induced an increased CD absorption at 222 nm, which initially suggested the formation of heterodimeric helical coiled coils (*18*). However, a similar spectrum has been also characterized for a pure component of type I β-turns in cyclic model peptides (*39*). The appearance of a prominent IR band at 1675−1678 cm^{-1}, assigned to β-turn structures (*27*, *28*), would support the idea that this conformation also dominates the hybK3 CD spectrum recorded in 5% HFIP. Two-dimensional IR correlation data indicated that HFIP-induced changes in the β-turn and β-sheet regions precede helix formation, which did not predominate until 25 or 50% HFIP. In summary, our combined CD and IR structural data established a correlation between the enhancement of FP recognition by MAb2F5 and stabilization of the nonhelical β-turn and β-sheet AIS structure.

Implications for gp41 Structure and Function. The AIS region is predicted to be dynamic and to alternate between at least two stable conformations in the fusion pathway: (i) the Fab2F5-bound nonhelical structure in prefusion gp41 (*17*, *23*) and (ii) the amphipathic helix extending α-helices from the preceding CHR region while partially immersed at the water−membrane interface (*14*). We propose that in the gp41 refolding pathway, assembly of the FP−AIS complex might act as a kinetic trap that locks the AIS region into the nonhelical conformation recognized by the antibody. In line with this, we propose that in the gp41 prefusion state FP−AIS interactions might augment the solubility of the FP residues, thereby preventing their insertion into the viral membrane (model in Figure 9). Our data actually suggest that as a result of FP−AIS interactions, the capacity of FP to perturb membranes would be impaired.

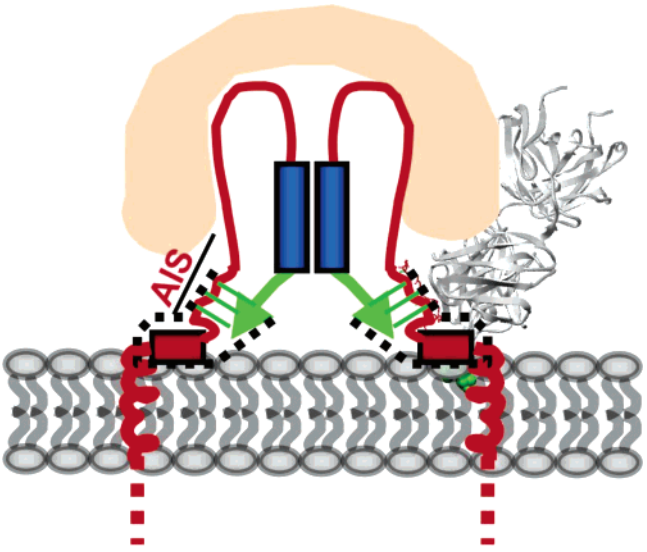

FIGURE 9: Model proposed for the organization of native gp41 in the virion membrane (only one gp41 dimer is shown for visual clarity). FP (green arrow) and AIS (folded stretch in red bound by Fab2F5 in gray ribbons) are postulated to assemble into a complex in the prefusion gp41 ectodomain. The NHR helix is represented by the blue cylinder. The structure of the sequence connecting the NHR with AIS is unknown (red loop). The small red cylinder inserted into the membrane interface designates the preTM domain stretch not bound by mAb2F5. AIS, FP, and preTM comprise the structural elements included within the Env foot (*17*) (broken line). The Fab2F5−AIS (*23*) ribbon model was derived from the atomic structure with Protein Data Bank entry 1TJI and rendered with Swiss-PDBviewer.

Our study further suggests that the structure of the FP−AIS complex might be affected by polarity gradients. This observation might be relevant given the virion Env organization revealed by cryoelectron microscopy tomography (*17*), which situates the preTM domain inserted in parallel into the interface of the external monolayer of the viral membrane (see the cartoon in Figure 9). IR analyses revealed that a reduction in polarity increased the turn content and diminished the β-sheet content (Figures 5 and 6). Moreover, asynchronous maps based on the deconvolved spectra suggested that 3_{10}-helices might follow sheets and turns during the HFIP-induced transition (Figure 6). Thus, "stretched" 3_{10}-helices might comprise intermediate structures between type I β-turns and α-helices. Interestingly, the 3_{10}-

helix conformation has been demonstrated to be distinctively accessible to the AIS region (*34*). This order of events also supports the idea that a β-turn-like conformation may serve as a conformational template for the formation of helical structure (*51*).

We speculate that the FP−AIS complex disassembles concomitantly with the adoption of α-helical structure in the low-polarity medium. This assumption is supported by the fact that α-helix formation occurs at high HFIP contents, and it is accompanied by an increment in disorder. Thus, we surmise that an increase in the propensity to form helices sustained by the low polarity of the interfacial region might help in the dissociation of the FP−AIS complex at the foot's instep−heel gp41 region. Monomeric, stable structures of the FP adopting a main helical conformation have been determined in low-polarity environments (*30*, *31*). In this way, the membrane−interface partitioning−folding coupling might play a role in bundle formation, facilitating the extension of the CHR helices. Growth and completion of the 6-HB while it is connected to the membrane seem to be important for concomitant opening of a fusion pore (*8*, *14*, *52*).

ACKNOWLEDGMENT

We are grateful to F. M. Goñi, for critical reading of the manuscript and to G. Basañez, A. Muga, and A. R. Viguera for fruitful discussions. We also thank Drs. David Weliky and Jun Yang for the initial supply of FPK3.

REFERENCES

1. Doms, R. W., and Moore, J. P. (2000) HIV-1 membrane fusion: Targets of opportunity, *J. Cell Biol. 151*, F9−F14.
2. Eckert, D. M., and Kim, P. S. (2001) Mechanisms of viral fusion and its inhibition, *Annu. Rev. Biochem. 70*, 777−810.
3. Gallo, S. A., Finnegan, C. M., Viard, M., Raviv, Y., Dimitrov, A., Rawat, S. S., Puri, A., Durell, S., and Blumenthal, R. (2003) The HIV Env-mediated fusion reaction, *Biochim. Biophys. Acta 1614*, 36−50.
4. Chan, D. C., Fass, D., Berger, J. M., and Kim, P. S. (1997) Core structure of gp41 from the HIV-1 envelope glycoprotein, *Cell 89*, 263−273.
5. Weissenhorn, W., Dessen, A., Harrison, S. C., Skehel, J. J., and Wiley, D. C. (1997) Atomic structure of the ectodomain from HIV-1 gp41, *Nature 387*, 426−428.
6. Furuta, R. A., Wild, C. T., Weng, Y., and Weiss, C. D. (1998) Capture of an early fusion-active conformation of HIV-1 gp41, *Nat. Struct. Biol. 5*, 276−279.
7. Muñoz-Barroso, I., Durell, S., Sakaguchi, K., Appella, E., and Blumenthal, R. (1998) Dilation of the human inmunodeficiency virus-1 envelope glycoprotein fusion pore revealed by the inhibitory action of a synthetic peptide from gp41, *J. Cell Biol. 140*, 315−323.
8. Melikyan, G. B., Markosyan, R. M., Hemmati, H., Delmedico, M. K., Lambert, D. M., and Cohen, F. S. (2000) Evidence that the transition of HIV-1 gp41 into a six-helix bundle, not the bundle configuration, induces membrane fusion, *J. Cell Biol. 151*, 413−423.
9. Nieva, J. L., and Agirre, A. (2003) Are fusion peptides a good model to study viral cell fusion? *Biochim. Biophys. Acta 1614*, 104−115.
10. Salzwedel, K., West, J., and Hunter, E. (1999) A conserved tryptophan-rich motif in the membrane-proximal region of the human immunodeficiency virus type 1 gp41 ectodomain is important for env-mediated fusion and virus infectivity, *J. Virol. 73*, 2469−2480.
11. Muñoz-Barroso, I., Salzwedel, K., Hunter, E., and Blumenthal, R. (1999) Role of the membrane-proximal domain in the initial stages of human immunodeficiency virus type 1 envelope glycoprotein-mediated membrane fusion, *J. Virol. 73*, 6089−6092.
12. Suárez, T., Gallaher, W. R., Agirre, A., Goñi, F. M., and Nieva, J. L. (2000) Membrane interface-interacting sequences within the ectodomain of the HIV-1 envelope glycoprotein: Putative role during viral fusion, *J. Virol. 74*, 8038−8047.
13. Sáez-Cirión, A., Nir, S., Lorizate, M., Agirre, A., Cruz, A., Pérez-Gil, J., and Nieva, J. L. (2002) Sphyngomyelin and cholesterol promote HIV-1 gp41 pretransmembrane sequence surface aggregation and membrane restructuring, *J. Biol. Chem. 277*, 21776−21785.
14. Sáez-Cirión, A., Arrondo, J. L. R., Gómara, M. J., Lorizate, M., Iloro, I., Melikyan, G., and Nieva, J. L. (2003) Structural and functional roles of HIV-1 gp41 pre-transmembrane sequence segmentation, *Biophys. J. 85*, 3769−3780.
15. Schibli, D. J., Montelaro, R. C., and Vogel, H. J. (2001) The membrane-proximal tryptophan-rich region of the HIV glycoprotein, gp41, forms a well-defined helix in dodecylphosphocholine micelles, *Biochemistry 40*, 9570−9578.
16. Shnaper, S., Sackett, K., Gallo, S. A., Blumenthal, R., and Shai, Y. (2004) The C- and the N-terminal regions of glycoprotein 41 ectodomain fuse membranes enriched and not enriched with cholesterol, respectively, *J. Biol. Chem. 279*, 18526−18534.
17. Zhu, P., Liu, J., Bess, J., Chertova, E., Lifson, J. D., Grisé, H., Ofek, G. A., Taylor, K. A., and Roux, K. H. (2006) Distribution and three-dimensional structure of AIDS envelope spikes, *Nature 44*, 847−852.
18. Lorizate, M., Gómara, M. J., de la Torre, B., Andreu, D., and Nieva, J. L. (2006) Membrane-transferring sequences of the HIV-1 gp41 ectodomain assemble into an immunogenic complex, *J. Mol. Biol. 360*, 45−55.
19. Muster, T., Steindl, F., Purtscher, M., Trkola, A., Klima, A., Himmler, G., Ruker, F., and Katinger, H. (1993) A conserved neutralizing epitope on gp41 of human immunodeficiency virus type 1, *J. Virol. 67*, 6642−6647.
20. Purtscher, M., Trkola, A., Gruber, G., Buchacher, A., Predl, R., Steindl, F., Tauer, C., Berger, R., Barrett, N., Jungbauer, A., et al. (1994) A broadly neutralizing human monoclonal antibody against gp41 of human immunodeficiency virus type 1, *AIDS Res. Hum. Retroviruses 10*, 1651−1658.
21. Parker, C. E., Deterding, L. J., Hager-Braun, C., Binley, J. M., Schulke, N., Katinger, H., Moore, J. P., and Tomer, K. B. (2001) Fine definition of the epitope on the gp41 glycoprotein of human immunodeficiency virus type 1 for the neutralizing monoclonal antibody 2F5, *J. Virol. 75*, 10906−10911.
22. Barbato, G., Bianchi, E., Ingallinella, P., Hurni, W. H., Miller, M. D., Ciliberto, G., Cortese, R., Bazzo, R., Shiver, J. W., and Pessi, A. (2003) Structural analysis of the epitope of the anti-HIV antibody 2F5 sheds light into its mechanism of neutralization and HIV fusion, *J. Mol. Biol. 330*, 1101−1115.
23. Ofek, G., Tang, M., Sambor, A., Kainger, H., Mascola, J. R., Wyatt, R., and Kwong, P. D. (2004) Structure and mechanistic analysis of the anti-human immunodeficiency virus type 1 antibody 2F5 in complex with its gp41 epitope, *J. Virol. 78*, 10724−10737.
24. Nieva, J. L., Nir, S., Muga, A., Goñi, F. M., and Wilschut, J. (1994) Interaction of the HIV-1 fusion peptide with phospholipid vesicles: Different structural requirements for leakage and fusion, *Biochemistry 33*, 3201−3209.
25. Ellens, H., Bentz, J., and Szoka, F. C. (1985) H^+- and Ca^{2+}-induced fusion and destabilization of liposomes, *Biochemistry 24*, 3099−3106.
26. Hoekstra, D., De Boer, T., Klappe, K., and Wilschut, J. (1984) Fluorescence method for measuring the kinetics of fusion between biological membranes, *Biochemistry 23*, 5675−5681.
27. Arrondo, J. L. R., Muga, A., Castresana, J., and Goñi, F. M. (1993) Quantitative studies of the structure of proteins in solution by Fourier-transformed infrared spectroscopy, *Prog. Biophys. Mol. Biol. 59*, 23−56.
28. Arrondo, J. L. R., and Goñi, F. M. (1999) Structure and dynamics of membrane proteins as studied by infrared spectroscopy, *Prog. Biophys. Mol. Biol. 72*, 367−405.
29. Turnay, J., Olmo, N., Gasset, M., Iloro, I., Arrondo, J. L. R., and Lizarbe, M. A. (2002) Calcium-dependent conformational rearrangements and protein stability in chicken annexin A5, *Biophys. J. 83*, 2280−2291.
30. Gordon, L. M., Mobley, P. W., Pilpa, R., Sherman, M. A., and Waring, A. J. (2002) Conformational mapping of the N-terminal peptide of HIV-1 gp41 in membrane environments using ^{13}C-enhanced Fourier transform infrared spectroscopy, *Biochim. Biophys. Acta 1559*, 96−120.

31. Jaroniec, C. P., Kaufman, J. D., Stahl, S. J., Viard, M., Blumenthal, R., Wingfield, P. T., and Bax, A. (2005) Structure and dynamics of micelle-associated human immunodeficiency virus gp41 fusion domain, *Biochemistry 44*, 16167−16180.
32. Stiegler, G., Kunert, R., Purtscher, M., Wolbank, S., Voglauer, R., Steindl, F., and Katinger, H. (2001) A potent cross-clade neutralizing human monoclonal antibody against a novel epitope on gp41 of human immunodeficiency virus type 1, *AIDS Res. Hum. Retroviruses 17*, 1757−1765.
33. Pereira, F. B., Goñi, F. M., and Nieva, J. L. (1995) Liposome destabilization induced by the HIV-1 fusion peptide. Effect of a single amino acid substitution, *FEBS Lett. 362*, 243−246.
34. Biron, Z., Khare, S., Samson, A. O., Hayek, Y., Naider, F., and Anglister, J. (2002) A monomeric 3_{10}-helix is formed in water by a 13-residue peptide representing the neutralizing determinant of HIV-1 on gp41, *Biochemistry 41*, 12687−12696.
35. Greenfield, N. J. (1996) Methods to estimate the conformation of proteins and polypeptides from circular dichroism data, *Anal. Biochem. 235*, 1−10.
36. Sreerama, N., and Woody, R. W. (2004) Computation and analysis of protein circular dichroism spectra, *Methods Enzymol. 383*, 318−351.
37. Keating, A. E., Malashkevich, V. N., Tidor, B., and Kim, P. S. (2001) Side-chain repacking calculations for predicting structures and stabilities of heterodimeric coiled coils, *Proc. Natl. Acad. Sci. U.S.A. 98*, 14825−14830.
38. Litowski, J. R., and Hodges, R. S. (2002) Designing heterodimeric two-stranded α-helical coiled-coils. Effects of hydrophobicity and α-helical propensity on protein folding, stability, and specificity, *J. Biol. Chem. 277*, 37272−37279.
39. Perczel, A., and Fasman, G. D. (1992) Quantitative analysis of cyclic *β*-turn models, *Protein Sci. 1*, 378−395.
40. Perczel, A., and Hollósi, M. (1996) Turns, in *Circular Dichroism and the Conformational Analysis of Biomolecules* (Fasman, G. D., Ed.) pp 285−380, Plenum Press, New York.
41. Noda, I., Dowrey, A. E., Marcott, C., Story, G. M., and Ozaki. Y. (2000) Generalized two-dimensional correlation spectroscopy, *Appl. Spectrosc. 54*, 236A−248A.
42. Arrondo, J. L. R., Iloro, I., Aguirre, J., and Goñi, F. M. (2004) A two-dimensional IR spectroscopic (2D-IR) simulation of protein conformational changes, *Spectroscopy 18*, 49−58.
43. Iloro, I., Chehin, R., Goñi, F. M., Pajares, M. A., and Arrondo, J. L. (2004) Methionine adenosyltransferase α-helix structure unfolds at lower temperatures than *β*-sheet: A 2D-IR study, *Biophys. J. 86*, 3951−3958.
44. Kennedy, D. F., Crisma, M., Toniolo, C., and Chapman, D. (1991) Studies of peptides forming 3_{10}- and α-helices and *β*-bend ribbon structures in organic solution and in model biomembranes by Fourier transform infrared spectroscopy, *Biochemistry 30*, 6541−6548.
45. Silva, R. A., Yasui, S. C., Kubelka, J., Formaggio, F., Crisma, M., Toniolo, C., and Keiderling, T. A. (2002) Discriminating 3_{10}-from α-helices: Vibrational and electronic CD and IR absorption study of related Aib-containing oligopeptides, *Biopolymers 65*, 229−243.
46. Toniolo, C., Formaggio, F., Tognon, S., Broxterman, Q. B., Kaptein, B., Huang, R., Setnicka, V., Keiderling, T. A., McColl, I. H., Hecht, L., and Barron, L. D. (2004) The complete chirospectroscopic signature of the peptide 3_{10}-helix in aqueous solution, *Biopolymers 75*, 32−45.
47. McGaughey, G. B., Citron, M., Danzeisen, R. C., Freidinger, R. M., Garsky, V. M., Hurni, W. M., Joyce, J. G., Liang, X., Miller, M., Shiver, J., and Bogusky, M. J. (2003) HIV-1 vaccine development: Constrained peptide immunogens show improved binding to the anti-HIV-1 gp41 MAb, *Biochemistry 42*, 3214−3223.
48. Tian, Y., Ramesh, C. V., Ma, X., Naqvi, S., Patel, T., Cenizal, T., Tiscione, M., Diaz, K., Crea, T., Arnold, E., Arnold, G. F., and Taylor, J. W. (2002) Structure-affinity relationships in the gp41 ELDKWA epitope for the HIV-1 neutralizing monoclonal antibody 2F5: Effects of side-chain and backbone modifications and conformational constraints, *J. Pept. Res. 59*, 264−276.
49. Zwick, M. B., Jensen, R., Church, S., Wang, M., Stiegler, G., Kunert, R., Katinger, H., and Burton, D. R. (2005) Anti-human immunodeficiency virus type 1 (HIV-1) antibodies 2F5 and 4E10 require surprisingly few crucial residues in the membrane-proximal external region of glycoprotein gp41 to neutralize HIV-1, *J. Virol. 79*, 1252−1261.
50. Joyce, J. G., Hurni, W. M., Bogusky, M. J., Garsky, V. M., Liang, X., Citron, M. P., Danzeisen, R. C., Miller, M. D., Shiver, J. W., and Keller, P. M. (2002) Enhancement of α-helicity in the HIV-1 inhibitory peptide DP178 leads to an increased affinity for human monoclonal antibody 2F5 but does not elicit neutralizing responses in vitro. Implications for vaccine design, *J. Biol. Chem. 277*, 45811−45820.
51. Perczel, A., Foxman, B. M., and Fasman, G. D. (1992) How reverse turns may mediate the formation of helical segments in proteins: An X-ray model, *Proc. Natl. Acad. Sci. U.S.A. 89* (17), 8210−8214.
52. Melikyan, G. B., Egelhofer, M., and von Laer, D. (2006) Membrane-anchored inhibitory peptides capture human immunodeficiency virus type 1 gp41 conformations that engage the target membrane prior to fusion, *J. Virol. 80*, 3249−3258.
53. Sreerama, N., and Woody, R. W. (2000) Estimation of protein secondary structure from circular dichroism spectra: Comparison of CONTIN, SELCON, and CDSSTR methods with an expanded reference set, *Anal. Biochem. 287*, 252−260.
54. Wimley, W. C., and White, S. H. (1996) Experimentally determined hydrophobicity scale for proteins at membrane interfaces, *Nat. Struct. Biol. 3*, 842−848.
55. Choisy, M., Woelk, C. H., Guégan, J., and Robertson, D. L. (2004) Comparative study of adaptive molecular evolution in different human immunodeficiency virus groups and subtypes, *J. Virol. 78*, 1962−1970.

BI0612521